https://doi.org/10.5194/egusphere-2026-1596
Preprint. Discussion started: 1 April 2026

Fault and fracture networks as long-lived conduits for lithium transport

Adam J. Cawood[1], David A. Ferrill[1], Isaac A. Rangel-Landeros[2], Kristina L. Butler[2], Daniel E. Ibarra[3,4], Zachary T. Sickmann[2], Madigan R. Blake[2], Brandon Swanson[5], Kevin J. Smart[1], Lee Ann Munk[6,7], David F. Boutt[8], Lisa D. Stockli[9], Daniel F. Stockli[9], and Catherine A. Gagnon[3,4]

[1]Southwest Research Institute, 6220 Culebra Rd., San Antonio, Texas, 78238, USA
[2]Department of Sustainable Earth Systems Sciences, The University of Texas at Dallas, Richardson, Texas 75080, USA
[3]Department of Earth, Environmental and Planetary Sciences, Brown University, Providence, Rhode Island 02912, USA
[4]Institute at Brown for Environment and Society, Brown University, Providence, Rhode Island 02912, USA
[5]Albemarle Corporation, NV-265, Silver Peak, Nevada, 89047, USA
[6]Department of Geosciences, University of Alaska Fairbanks, 308 Reichardt Bldg., 1930 Yukon Dr., Fairbanks, AK 99775, USA
[7]Geophysical Institute, University of Alaska Fairbanks, 2156 Koyukuk Dr., Fairbanks, AK, 99775, USA
[8]Department of Earth, Geographic, and Climate Sciences, University of Massachusetts Amherst, Amherst, Massachusetts 01003, USA
[9]Jackson School of Geosciences, University of Texas, Austin, TX, 78712-1722, USA

Correspondence to: Adam J. Cawood (adam.cawood@swri.org)

Abstract. Lithium brine systems are critical resources for the energy transition, yet the mechanisms governing lithium mobilization, transport, and concentration remain poorly constrained. In particular, the role of fault and fracture networks in controlling fluid flow and lithium distribution is not well resolved. Here we investigate the structural controls on lithium transport in Clayton Valley, Nevada, a key lithium-producing basin in the USA. We present new analyses of calcite-mineralized faults, opening-mode fractures, and spring deposits that record lithium-bearing fluid flow over >10 Myr of Basin and Range extension. Hereafter, opening-mode fractures are referred to as "fractures," and mineral-cemented faults or fractures as "veins." Calcite U–Pb ages (15–4 Ma), clumped-isotope formation temperatures (25–140 °C), and lithium concentrations (up to 460 ppm) demonstrate that fault and fracture networks repeatedly transported lithium-bearing fluids through basement, along basin margins, and within basin fill throughout basin evolution. Lithium concentrations vary systematically with host setting, with the highest values recorded in basin-fill-hosted veins and spring deposits and generally lower values in basement-hosted and basin-bounding fault veins. Several lithium-bearing calcite veins yield U–Pb ages that predate emplacement of late Miocene silicic volcanic units by up to ~9 Myr, demonstrating that structurally focused lithium transport occurred prior to emplacement of widely cited volcanic source reservoirs. Temperature and stable isotope constraints indicate dominantly meteoric fluids advected to depth and focused along faults, suggesting that lithium transport and enrichment in Clayton Valley does not necessarily require ascent of lithium-enriched magmatic fluids along deeply rooted crustal-scale faults. These results show that long-lived fault and fracture networks act as persistent pathways for lithium transport and redistribution within closed extensional basins. Although fault-controlled lithium enrichment has been recognized previously, this study provides direct evidence for structurally focused lithium transport over multi-Myr timescales.

https://doi.org/10.5194/egusphere-2026-1596
Preprint. Discussion started: 1 April 2026

1 Introduction

Closed-basin brines host some of the world's largest continental lithium accumulations and play a central role in the global lithium supply (Bradley et al., 2017; Coffey et al., 2021). Formation of these systems requires the coincidence of suitable lithium sources, hydrologic or tectonic basin closure, arid climate, and basin-scale processes capable of mobilizing, transporting, and concentrating lithium over geologic timescales (Bradley et al., 2013; Munk et al., 2016, 2025). In basin-hosted lithium systems, lithium enrichment is commonly attributed to meteoric leaching of silicic volcanic rocks and ash, volcaniclastic basin fill, and, in some cases, deeper basement lithologies, followed by progressive concentration within evolving basin depocenters (Price et al., 2000; Coffey et al., 2021; Munk et al., 2016, 2025; Darin et al., 2025; Thompson et al., 2025).

At the deposit-model scale, *"active faulting appears to be involved in all lithium basins"* (Bradley et al., 2013), reflecting the role of tectonically driven subsidence and/or uplift in creating accommodation space and aquifer systems capable of hosting economic volumes of lithium-rich brines. Across tectonic settings, structural and tectonostratigraphic development (including basin formation) is accompanied by brittle deformation, during which fault and fracture networks form, link, and are reactivated through time (e.g., Hancock, 1985; Cawood et al., 2021; Ferrill et al., 2021). As a result, tectonically developed basins—including active lithium basins in both extensional and contractional regimes—are characterized by pervasive fault and fracture networks that exert a strong influence on subsurface structure and permeability (e.g., Bradley et al., 2013; Marazuela et al., 2020; Putzolu et al., 2025). Fault and fracture networks are therefore fundamental components of groundwater flow in these settings, exerting first-order controls on permeability, locally focusing or impeding fluid migration (e.g., Caine et al., 1996; Bense et al., 2013), enabling fluid flow within basins, and potentially providing pathways for interbasin-scale solute transport over tens of kilometers (e.g., Heilweil and Brooks, 2011; Munk et al., 2016).

Faults and fractures have been invoked as constructive pathways that promote lithium enrichment by focusing fluid flow, enhancing water–rock interaction, and linking deep and shallow reservoirs, particularly in volcano–sedimentary settings where hydrothermal alteration and lithium enrichment are spatially associated with structural zones (e.g., Bradley et al., 2013; Marazuela et al., 2020; Benson et al., 2023). Conversely, faults have also been proposed to facilitate fluid leakage, potentially compromising lithium retention by allowing solute-rich fluids to escape basin reservoirs (e.g., Watts, 2025). In most cases, these interpretations are based on spatial associations, and basin-scale hydrogeologic models, or brine geochemistry (Heilweil and Brooks, 2011; Coffey et al., 2021), rather than direct records of fluid flow along individual fault or fracture systems. Consequently, the timing, depth, and persistence of fault-controlled fluid circulation in active lithium basins remain insufficiently constrained.

A key limitation in evaluating the role of faults in lithium systems is the lack of direct constraints on fault-hosted fluid flow through time. Mineral veins precipitated within faults and fractures, and spring travertine deposits associated with faults at depth, provide direct geochemical records of fluids that circulated along discrete structures (Fyfe et al., 1978; Eaton, 1982;

https://doi.org/10.5194/egusphere-2026-1596
Preprint. Discussion started: 1 April 2026

Chen et al., 2024). Such records have not (to our knowledge) been directly constrained by absolute geochronology of structural pathways in active lithium basins, however. Here, we analyze calcite veins hosted in faults and fractures, together with spring and travertine deposits interpreted to reflect structurally focused fluid flow, from the vicinity of the Silver Peak lithium mine in Clayton Valley, Nevada. We integrate U–Pb calcite geochronology, clumped-isotope thermometry, and lithium geochemistry to directly constrain the timing, depth, and geochemical character of fluids circulating along brittle structures during Basin and Range extension. Our approach evaluates the role of faults and fractures as pathways for lithium-bearing fluids within an active closed-basin lithium system, providing new constraints on the processes that link deformation, fluid flow, and lithium redistribution through time.

2 Geologic Setting

Clayton Valley is an extensional basin in the central Basin and Range province of western Nevada, located along the eastern margin of the Walker Lane belt (**Fig. 1a**). Clayton Valley is flanked by uplifted and faulted Proterozoic to Paleozoic basement rocks and overlain by Miocene and younger volcanic and volcaniclastic units associated with regional magmatism in the central Basin and Range province (**Fig. 1b, 1c**). Extension in Clayton Valley initiated at ca. 16 Ma via detachment faulting in the Silver Peak-Lone Mountain extensional complex and initiation of the Mineral Ridge detachment system (Stewart and Diamond, 1990; Oldow et al., 1994; Diamond and Ingersoll, 2002) which occupies an extensional structural stepover linking right-lateral strike slip faults of the Furnace Creek fault system with the central Nevada Walker Lane fault network (Oldow et al., 2009). Extension on this system was accompanied by upper-plate extension and exhumation of lower-plate rocks (Stewart and Diamond, 1990; Diamond and Ingersoll, 2002). By ~10–6 Ma, detachment activity waned and deformation localized onto higher-angle normal faults, coincident with half-graben development, focused subsidence, and late-Miocene silicic volcanism that emplaced key lithium-source materials (Cawood et al., 2025; Rangel et al., 2025; Darin et al., 2025).

https://doi.org/10.5194/egusphere-2026-1596
Preprint. Discussion started: 1 April 2026

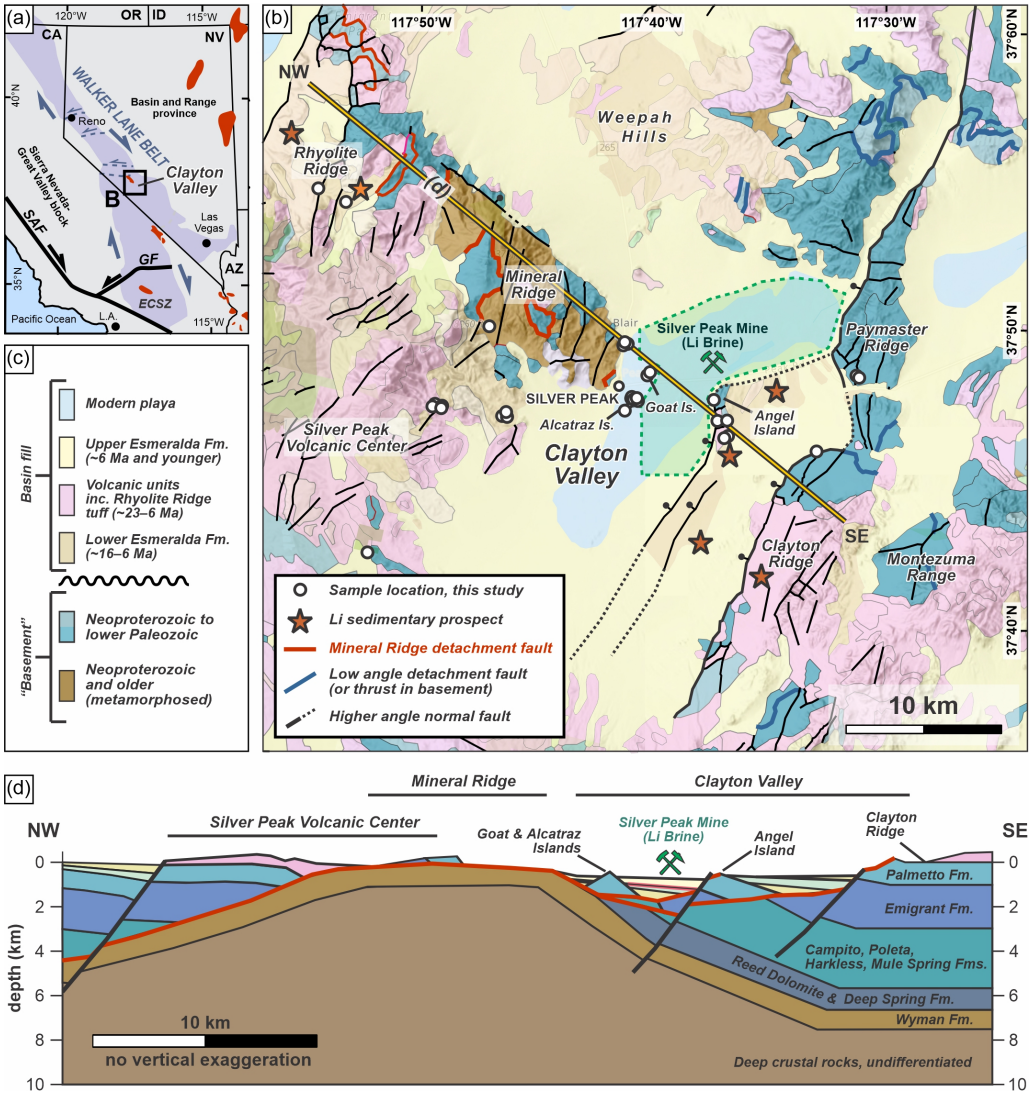

Figure 1. Geologic map of Clayton Valley, Nevada. (a) Regional tectonic provinces of the southwestern United States, adapted from Darin et al., 2025. Red polygons mark the position of exposed metamorphic core complexes in the region, including the Mineral Ridge detachment system in Clayton Valley; modified from Davis et al., 2023. (b) Geologic map of the greater Clayton Valley region, modified from Albers and Stewart (1972), U.S. Geological Survey (2024), and Darin et al. (2025). (c) Generalized stratigraphy. Formation names and approximate ages after Diamond and Ingersoll (2002). (d) NW-SE cross section across study area (location shown in part b).

Early Miocene slip on the Mineral Ridge detachment likely produced a broad basin filled by lower Esmeralda Formation strata, sourced from eastern and western highlands (Stewart and Diamond, 1990; Diamond and Ingersoll, 2002). Ongoing extension, including relatively recent deformation from the late Miocene onwards (~6 Ma and younger), generated west-dipping, higher-angle normal faults that localized Pliocene–Pleistocene lacustrine and volcaniclastic sedimentation and controlled accommodation space for volcano-sedimentary units (**Fig. 1d**; Cawood et al., 2025; Rangel et al., 2025). Basin fill comprises

https://doi.org/10.5194/egusphere-2026-1596
Preprint. Discussion started: 1 April 2026

interbedded tuffs, ash layers, lacustrine deposits, conglomerates, and sandstones, producing a heterogeneous stratigraphy that thickens eastward into fault-bounded sub-basins (Stewart and Diamond, 1990; Diamond and Ingersoll, 2002).

Lithium enrichment in Clayton Valley reflects the combined influence of basin structure, volcanic input, and hydroclimate evolution (Coffey et al., 2021; Gagnon et al., 2023; Bhattacharya et al., 2024). Basin fill comprises lithium-enriched volcaniclastic strata, lacustrine mudstones, and evaporite deposits (20–2000 ppm Li; Coffey et al., 2021), and brines that collectively host one of the world's largest continental lithium accumulations (Kunasz, 1974; Davis and Vine, 1979; Davis et al., 1986; Price et al., 2000; Gagnon et al., 2023; Bhattacharya et al., 2024). Early studies linked lithium brines to silicic volcanic centers, identifying volcanic glass and ash as primary lithium sources (Price et al., 2000). Subsequent work indicated that volcanogenic inputs are supplemented by complex basin-scale hydrologic mixing involving shallow meteoric waters and deeper basin fluids (Munk et al., 2011). Basin-fill clays and tuffs contain elevated lithium concentrations (20–2000 ppm), with up to ~30% of the lithium present in soluble form, and total basin inventories of 24–58 Mt of lithium stored in sediment and brine (Coffey et al., 2021). Basin architecture governs both routing and storage of lithium, and prior studies have conceptualized multiple end-member pathways for lithium transport within Clayton Valley, including interbasin inflow, intrabasin volcanogenic and sediment leaching and redistribution, and deeper basin-scale fluid circulation (e.g., Munk et al., 2016; Coffey et al., 2021).

3 Materials and Methods

3.1 Field work and sample collection

Thirty calcite-bearing samples were collected in and around Clayton Valley, Nevada (**Figs. 1, 2**). These include 15 calcite vein samples hosted in basement rocks, two samples from basin-bounding faults, nine calcite vein samples hosted within basin-fill strata, and four travertine samples associated with fossil carbonate spring deposits. Sampling of fault- and fracture-hosted calcite veins deliberately targeted relatively late-stage brittle structures interpreted to be related to Basin and Range extension, while avoiding earlier vein sets and fracture arrays (e.g., en echelon tension gashes) preserved in the basement. For these structures, strike and dip were measured at each site, with slip rake and displacement recorded where preserved (**Supplemental Material 1**). Sampling locations were selected to capture a range of structural settings and positions within and adjacent to the Clayton Valley. Travertine samples were collected from surface carbonate mounds developed on the basin floor and are not associated with active spring discharge, although some of these springs were active as recently as the mid 1900's prior to lithium brine production (Kunasz, 1974).

3.2 Analytical Methods

Compositional analysis was performed by ALS Geochemistry Testing and Analysis in Reno, Nevada using the *ME-MS89L Super Trace* inductively coupled plasma mass spectrometry (ICP-MS) method. Detection ranges for this method are reported

https://doi.org/10.5194/egusphere-2026-1596
Preprint. Discussion started: 1 April 2026

130 at ~2-25,000 parts per million (ppm) for lithium and other trace elements (ALS, 2025). All 30 of the calcite samples described in section 3.1 were analyzed for trace element composition.

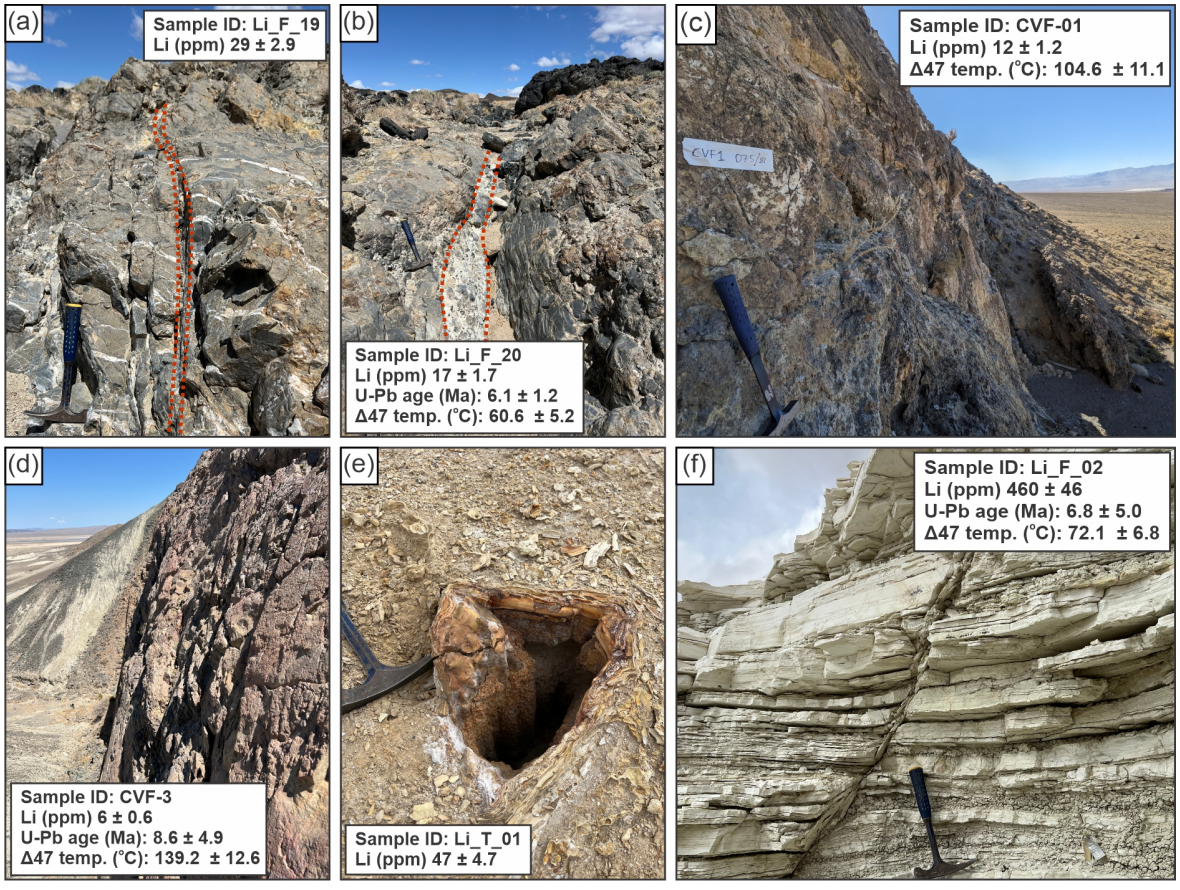

Figure 2. Sample types and settings collected for geochemical analysis. (a) Basement-hosted opening-mode vein; view to the north. (b) Basement-hosted normal fault with cemented breccia fill; view to the north (c) Basin-bounding fault at west side of Clayton 135 **Ridge; view to the south. (d) Major fault on the west flank of Angel Island; view to the north; fault scarp is ca. 15 m high. (e) Paleo–hot spring deposit associated with fault-controlled fluid discharge and spring precipitation. (f) Calcite-mineralized fault hosted within basin-fill sediments; view to the north. Red dotted lines in parts a and b delineate structure sampled. Note, in both a and b sampled structures strike approximately N-S and cut across older veins in basement units.**

U–Pb calcite geochronology was conducted at the UTChron Laboratory, University of Texas at Austin, using in situ laser 140 ablation ICP-MS methods. Analyses included petrographic characterization and screening for uranium content prior to dating. Calcite veins were analyzed as thick sections (~60 µm), with approximately 40 ablation spots per sample, following the protocols of Palacios-García et al. (2023). Measurements were performed using a high-resolution magnetic-sector ICP-MS coupled to a 193 nm excimer laser. Data reduction and age calculations were performed using Iolite4 (Paton et al., 2011) with the VisualAge UcomPbine data reduction scheme (Chew et al., 2014). A ^{207}Pb-based common-Pb correction was applied using 145 the primary calcite reference material WC-1 (Roberts and Walker, 2016; Roberts et al., 2017). Elemental and isotopic fractionation were corrected through interspersed analyses of WC-1, secondary calcite reference material RA138, and NIST-

https://doi.org/10.5194/egusphere-2026-1596
Preprint. Discussion started: 1 April 2026

614 glass (Hollocher and Ruiz, 1995; Jochum et al., 2005; Kaiyun et al., 2014). Secondary reference material RA138 yielded a mean $^{206}Pb/^{238}U$ age of 308 ± 4 Ma (MSWD = 4.5; n = 109), consistent with published values (Guillong et al., 2024). U–Pb data were plotted on Tera–Wasserburg diagrams (Tera and Wasserburg, 1972), and lower-intercept ages were calculated using IsoplotR (Vermeesch, 2018). In total, 18 samples were analyzed for U–Pb geochronology.

Carbonate clumped isotope thermometry was conducted at Brown University. Each sample (~50 mg, depending on carbonate content) was reacted with 104% orthophosphoric acid at 90°C for 20 minutes and the resulting CO_2 was continuously frozen in liquid N_2 throughout the reaction. Cryogenic and gas chromatographic separations were conducted using the Protium Isotopologue Batch Extraction (IBEX) system to purify the gas before introduction into a Thermo MAT 253 Plus dual-inlet isotope ratio mass spectrometer. Carbonate isotopic clumping was quantified to estimate calcite crystallization temperatures using the Δ_{47} parameter [$\Delta_{47} = (R_{47} / R^*_{47} - 1) \times 1{,}000$], where R_{47} represents the measured abundance of mass 47 isotopologues relative to mass 44 in CO_2, and R^*_{47} is the expected stochastic distribution (Ghosh et al., 2006). Measured δ_{45}, δ_{46}, and δ_{47} values are corrected to $\delta^{13}C$, $\delta^{18}O$, and Δ_{47} using the calibration parameters of Brand et al. (2010), following the procedures of Daëron et al. (2016). Raw Δ_{47} values were projected onto the carbon dioxide equilibrium scale and $\delta^{13}C$ and $\delta^{18}O$ values were corrected using the ETH1–3 carbonate standard (Bernasconi et al., 2021). Calcite calibrations of Anderson et al. (2021) were used to translate Δ_{47} values into temperature estimates and measurement uncertainties were quantified and propagated through Monte Carlo simulations to ensure reliable error estimates.

4 Results

Measured lithium concentrations in fault- and fracture-hosted calcite veins and spring deposit carbonates range from below detection limits (<2 ppm; ALS, 2025) to 460 ppm (**Figs. 3a, 4a, and 5**). Four of the 30 samples analyzed yielded lithium concentrations below detection limits, all of which are faults and fracture samples within Proterozoic to Paleozoic basement units (**Table 1**). For basement-hosted faults and fractures with measurable lithium, concentrations range from 3 to 29 ppm (median = 6 ppm; n = 11). Calcite veins in volcano-sedimentary basin-fill units exhibit the greatest variability in lithium concentrations, ranging from 3 to 460 ppm (median = 16 ppm; n = 9). Travertine and spring deposits yield consistently elevated lithium concentrations (13 to 112 ppm; median = 68.5 ppm; n = 4) relative to most vein calcites. Samples from basin-bounding faults contain comparatively low lithium concentrations (6–12 ppm; median = 9 ppm; n = 2). The full suite of bulk geochemistry data is provided in **Supplemental Material item 1.**

https://doi.org/10.5194/egusphere-2026-1596
Preprint. Discussion started: 1 April 2026

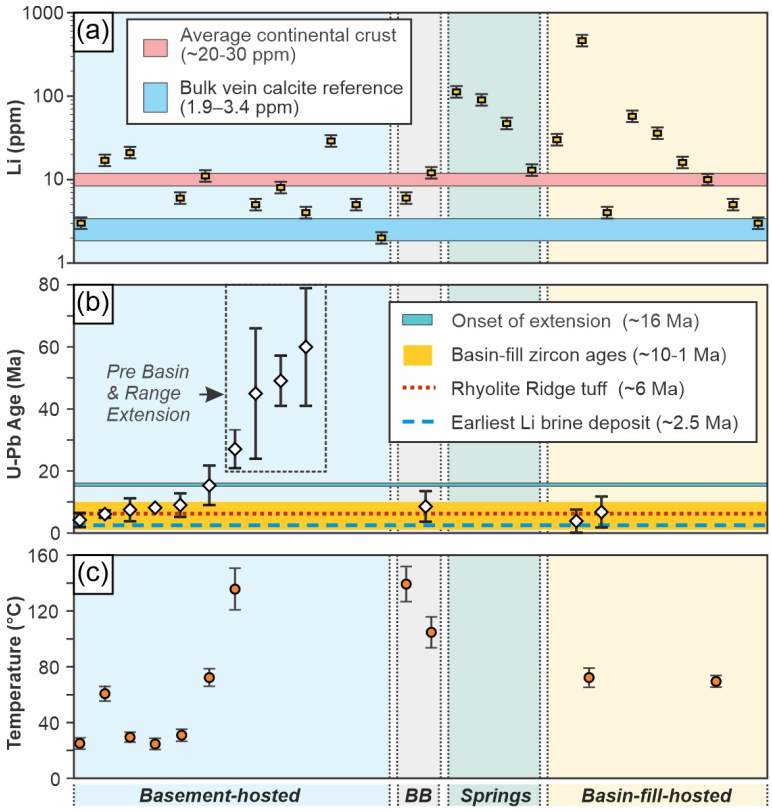

Figure 3. Geochemical data for calcite veins and travertine spring deposits. (a) Lithium concentrations (ppm); vertical error bars represent ±10% analytical uncertainty (ALS, 2025). Horizontal reference bars show average continental crust lithium concentrations (Watts, 2025) and published bulk vein calcite lithium concentrations (Drake et al., 2018). (b) U–Pb calcite ages (Ma); vertical error bars indicate 2σ uncertainty. Horizontal bars indicate onset of Basin and Range extension in the Clayton Valley-Silver Peak region (Diamond and Ingersoll, 2002), basin-fill zircon ages (Rangel et al., 2025), the Rhyolite Ridge tuff (Darin et al., 2025), and earliest halite deposition in Clayton Valley (Coffey et al., 2021; Gagnon et al., 2023). Ages older than the onset of Basin and Range extension (~25 Ma; Stewart, 1998) are highlighted. (c) Clumped-isotope temperatures (°C); vertical error bars represent 1σ uncertainty. Shaded vertical bands in panels A–C indicate sample setting; BB = basin-bounding faults.

Clumped-isotope (Δ47) and stable isotope analyses were performed on a subset of fault- and fracture-hosted calcite samples, including vein calcite and travertine deposits (**Figs. 3c, 4c, and 5**). Reconstructed carbonate precipitation temperatures span from ~25 to 139 °C across the dataset. Calcite hosted on basin-bounding faults records two elevated temperatures of 104.6 °C and 139.2 °C. Calcite veins hosted in volcano–sedimentary units yield two closely similar precipitation temperatures of 72.1 °C and 72.2 °C. Calcite mineralization hosted in basement faults and fractures, including travertine vein fill, spans the widest range of temperatures, with low-temperature values of ~25–31 °C, an intermediate value of 60.6 °C, and a high-temperature value of 135.6 °C. Carbonate $\delta^{13}C$ values range from +3.4 to −1.2‰ (VPDB), and carbonate $\delta^{18}O$ values range from −22.7 to −7.4‰ (VPDB). Calculated fluid $\delta^{18}O$ values span +7.8 to −13.9‰ (VSMOW) (**Fig. 6a**). Clumped-isotope formation temperatures exhibit a positive relationship with U–Pb calcite ages, with higher temperatures recorded in older calcite generations (**Fig. 6b**). Stable isotope and clumped-isotope data, including Δ_{47} measurements and calculated fluid compositions, are provided in **Supplemental Material item 4**.

https://doi.org/10.5194/egusphere-2026-1596
Preprint. Discussion started: 1 April 2026

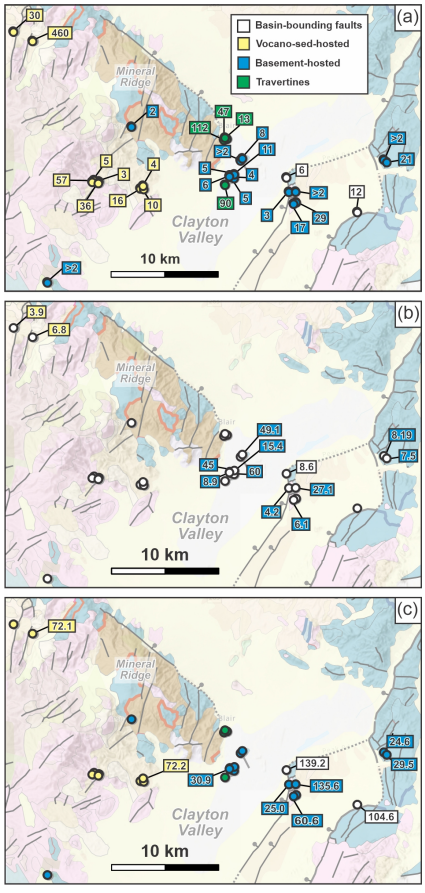

Figure 4. Spatial distribution of geochemical and geochronologic data from calcite veins and travertine deposits in and around Clayton Valley, Nevada. (a) Lithium concentrations in calcite (ppm). (b) U–Pb calcite ages (Ma). (c) Clumped-isotope calcite precipitation temperatures (°C). Symbols are color-coded by host setting (legend in panel a). Numeric labels indicate measured values for individual samples. See Fig. 1 for larger geologic context. These spatial data correspond to cross-plots and summary distributions presented in Fig. 3.

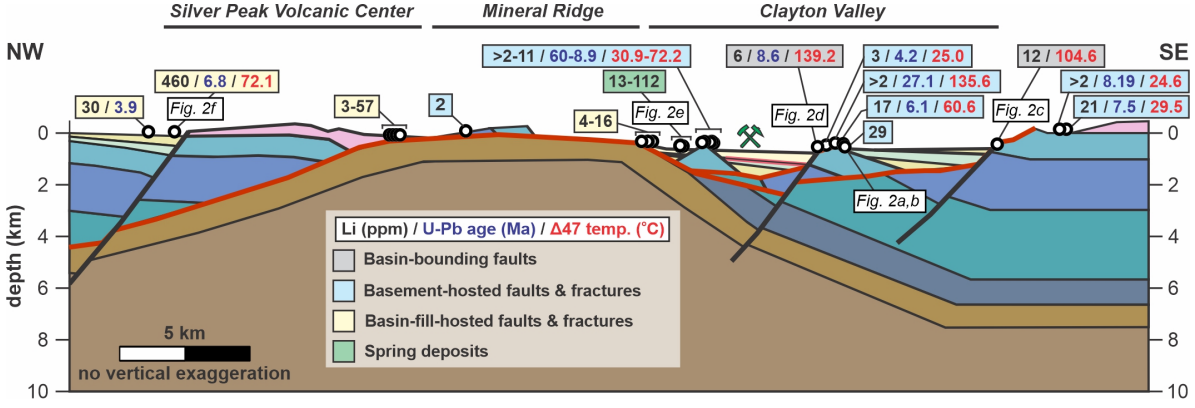

Figure 5. NW-SE cross section across study area (location shown in Fig. 1) showing projected sample locations and lithium concentrations, U-Pb ages, and clumped isotope temperatures. Modified from Cawood et al. (2025) and Rangel et al. (2025). Analytical uncertainties are omitted for clarity (see Fig. 3 and Supplemental Material item 1 for full suite of data and uncertainties).

https://doi.org/10.5194/egusphere-2026-1596
Preprint. Discussion started: 1 April 2026

U-Pb ages obtained from calcite mineralization span from 60 ± 19 Ma to 3.9 ± 3.7 Ma (**Figs. 3b, 4b, and 5**). Calcite mineralization hosted in faults and fractures within Proterozoic to Paleozoic basement rocks records the broadest range of ages, from 60 ± 19 Ma to 4.2 ± 2.3 Ma. The basin-bounding fault west of Angel Island (**Fig. 2d**) yields an age of 8.6 ± 4.9 Ma (**Fig. 5**). Veins hosted in volcano-sedimentary basin-fill units generally record younger ages, from 6.8 ± 5.0 Ma to 3.9 ± 3.7 Ma (**Table 1**). Several calcite samples did not yield robust U-Pb ages due to high proportions of common Pb. Travertine and spring deposits were not analyzed for U-Pb geochronology. U-Pb calcite geochronology data and associated Tera–Wasserburg plots are provided in **Supplemental Material items 2 and 3**.

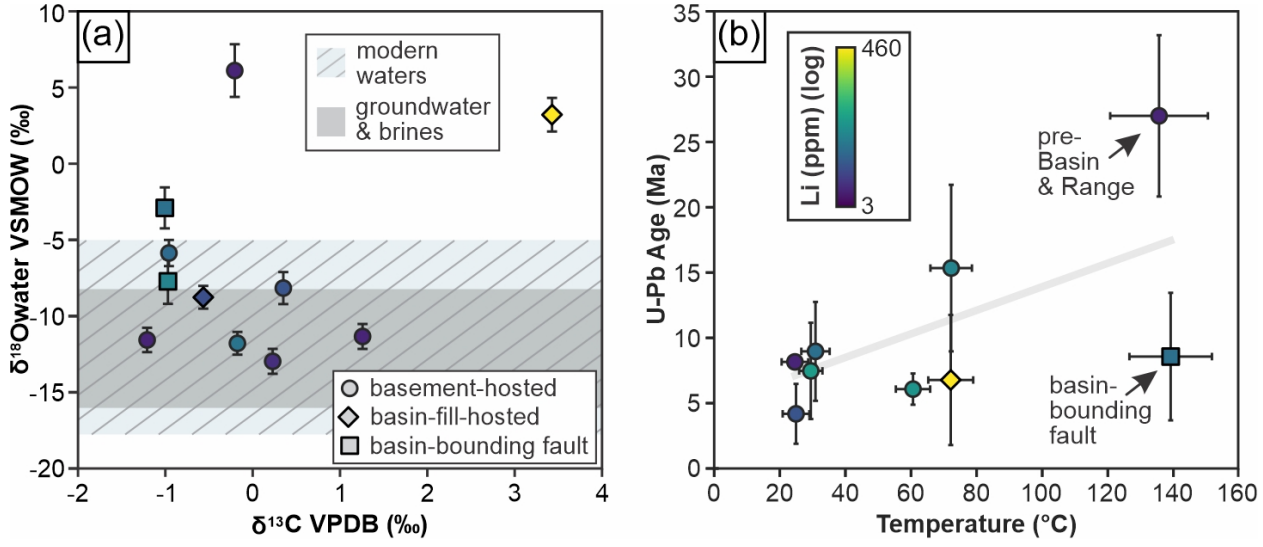

Figure 6. (a) Reconstructed fluid $\delta^{18}O$ (VSMOW) versus carbonate $\delta^{13}C$ (VPDB). Shaded fields show representative ranges of modern meteoric recharge and groundwater/brines for Clayton Valley (Gagnon et al., 2023). (b) U–Pb calcite age versus clumped-isotope temperature.

https://doi.org/10.5194/egusphere-2026-1596
Preprint. Discussion started: 1 April 2026

Table 1. Summary of samples and analytical results, ordered by geologic setting. Full dataset provided in Supplemental Material 1.

Sample	Setting	Structure	Li (ppm)	U-Pb Age (Ma)	δ13C VPDB (‰)	δ18O VPDB (‰)	δ18O VSMOW (‰)	Δ47 (I-CDES, ‰)	Temp. (°C)	δ18Owater VSMOW (‰)
Li_F_01	Basement	Dilational Normal Fault	2	--	--	--	--	--	--	--
Li_F_04	Basement	Opening-mode vein	8	49.1*	--	--	--	--	--	--
Li_F_05	Basement	Opening-mode vein	<2	--	--	--	--	--	--	--
Li_F_06	Basement	Normal Fault	11	15.4	0.34	-18.77	11.57	0.48	72.25	-8.24
Li_F_07	Basement	Fault, brecciated	6	9.0	0.22	-16.59	13.82	0.58	30.88	-13.07
Li_F_08	Basement	Opening-oblique-mode vein	5	45*	--	--	--	--	--	--
Li_F_09	Basement	Opening-mode vein	4	60*	--	--	--	--	--	--
Li_F_10	Basement	Opening-mode vein	5	--	--	--	--	--	--	--
Li_F_17	Basement	Fault, brecciated	<2	--	--	--	--	--	--	--
Li_F_18	Basement	Normal Fault	<2	27.1*	-0.21	-12.66	17.87	0.39	135.62	6.04
Li_F_19	Basement	Opening-mode vein	29	--	--	--	--	--	--	--
Li_F_20	Basement	Fault	17	6.1	-0.97	-14.71	15.75	0.51	60.61	-5.96
CVF-4	Basement	Opening-mode vein	3	4.2	1.25	-13.77	16.73	0.59	24.95	-11.41
CVF-5	Basement	Opening-mode vein	21	7.5	-0.18	-15.06	15.39	0.58	29.45	-11.82
CVF-6	Basement	Opening-mode vein	<2	8.2	-1.22	-13.91	16.58	0.60	24.61	-11.62
CVF-1	Basin-bounding	Normal Fault	12		-0.98	-22.68	7.54	0.43	104.61	-7.77
CVF-3	Basin-bounding	Normal Fault	6	8.6	-1.02	-21.84	8.40	0.38	139.16	-2.94
Li_T_01	Spring deposit	--	47	--	--	--	--	--	--	--
Li_T_02	Spring deposit	--	13	--	--	--	--	--	--	--
Li_T_03	Spring deposit	--	112	--	--	--	--	--	--	--
Li_T_04	Spring deposit	--	90	--	--	--	--	--	--	--
Li_F_02	Volcano-sedimentary	Normal Fault	460	6.8	3.43	-7.41	23.28	0.48	72.11	3.22
Li_F_03	Volcano-sedimentary	Normal Fault	30	3.9	--	--	--	--	--	--
Li_F_11	Volcano-sedimentary	Opening-mode vein	4	--	--	--	--	--	--	--
Li_F_12	Volcano-sedimentary	Opening-mode vein	16	--	--	--	--	--	--	--
Li_F_13	Volcano-sedimentary	Fault , oblique slip	57	--	--	--	--	--	--	--
Li_F_14	Volcano-sedimentary	Fault , oblique slip	5	--	--	--	--	--	--	--
Li_F_15	Volcano-sedimentary	Opening-mode vein	3	--	--	--	--	--	--	--
Li_F_16	Volcano-sedimentary	Opening-mode vein	36	--	--	--	--	--	--	--
CVF-2	Volcano-sedimentary	Opening-mode vein	10	--	-0.57	-18.98	11.35	0.49	69.51	-8.87

*U-Pb ages older than 25 Ma are interpreted to pre-date Basin and Range extension in study area. See main text for details

https://doi.org/10.5194/egusphere-2026-1596
Preprint. Discussion started: 1 April 2026

5 Discussion

5.1 Veins and spring deposits as tracers of lithium transport

Calcite veins and travertine spring deposits sampled here provide direct records of fluid chemistry at the time of mineralization (Fyfe et al., 1978; Eaton, 1982; Chen et al., 2024). These samples document lithium mobilization and transport by fluids circulating along faults and fractures in and around a basin that hosts one of the world's largest lithium accumulations (24–58 Mt; Coffey et al., 2021). Most samples contain measurable lithium across a wide concentration range, indicating that lithium was present in solution during fault- and fracture-hosted fluid flow at the time of vein and travertine formation. Although some calcite veins contain lithium concentrations below or near analytical detection limits (2 ppm), many samples yield values that exceed average upper continental crust concentrations (~30 ppm) and are substantially higher than lithium concentrations typically reported for calcite veins in non-mineralized systems (~1–5 ppm; Drake et al., 2018).

Calcite veins hosted within volcano-sedimentary basin-fill units exhibit the greatest range of lithium concentrations, including the highest measured values (up to 460 ppm). Travertine and spring deposits show consistently elevated lithium concentrations (13–112 ppm) relative to most fault- and fracture-hosted calcite veins. Elevated lithium concentrations in spring travertine deposits and basin-fill-hosted veins are interpreted to reflect fluid-rock interaction with lithium-enriched tuffaceous and sedimentary materials, and potentially local sourcing and remobilization of lithium from basin-fill into and along fractures. In contrast, basement-hosted calcite veins generally contain low to moderate lithium concentrations (commonly <10 ppm, rarely exceeding ~30 ppm), with several samples near or below analytical detection limits (2 ppm). Basin-bounding fault samples contain similarly low lithium concentrations (6 and 12 ppm). These lower lithium concentrations suggest that although circulation of lithium-bearing fluids through basement-rooted structures did occur, there was less lithium within these mineralizing fluids at the time of vein formation.

5.2 Timing, temperature, and chemistry of mineralizing fluids

Vein calcite precipitation ages associated with Basin and Range extension and basin development in Clayton Valley span ~15.4 to 3.9 Ma (**Figs. 4, 5, 7**), indicating that fluid flow and associated mineralization along faults and fractures persisted over multi-Myr timescales. These ages overlap both early activity of the Silver Peak–Lone Mountain detachment system (~16–6 Ma; Oldow et al., 1994, 2008) and later phases of deformation associated with development of the modern basin geometry (~6 Ma and younger; Rangel et al., 2025), highlighting the longevity of structurally controlled fluid pathways during basin evolution (**Fig. 7**). Coupled U–Pb ages and lithium concentrations in vein calcite demonstrate that lithium-bearing fluids were present and mobile throughout this extended period of extensional deformation, rather than being restricted to a narrow post-volcanic or post-depositional episode. Importantly, several of our lithium-bearing vein calcite samples yield ages that predate emplacement of silicic volcanic units that are commonly invoked as major lithium source reservoirs in the region, including ash-flow tuffs of the Montezuma Range (~7–8 Ma; Noble et al., 1964; Price et al., 2000) and the Rhyolite Ridge Tuff (~6 Ma; Darin et al., 2025). Lithium-bearing calcite precipitation prior to emplacement of these source units indicates that lithium

https://doi.org/10.5194/egusphere-2026-1596
Preprint. Discussion started: 1 April 2026

mineralization was therefore not solely tied to late Miocene volcanism and that lithium-bearing fluids were present within the evolving basin prior to eruption of these volcanic lithium-source units.

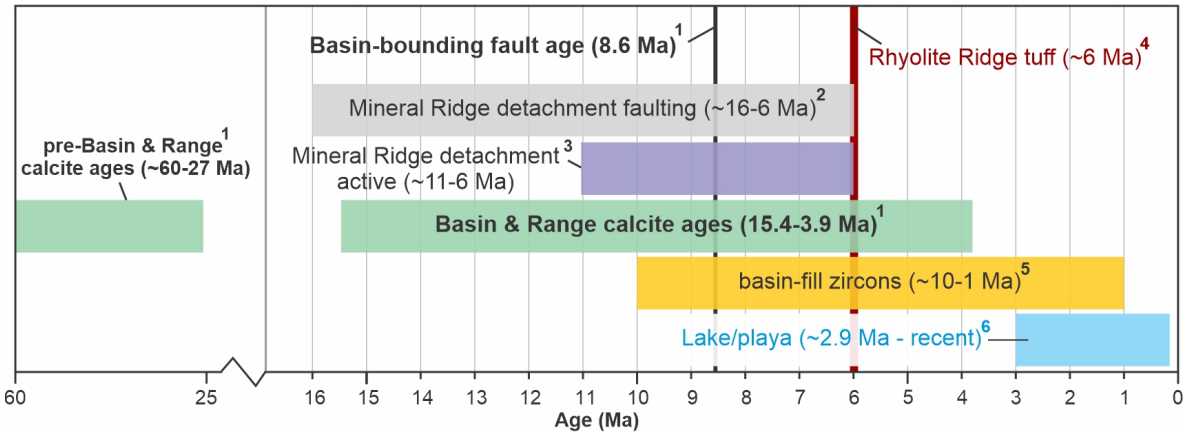

Figure 7. Time plot of U-Pb calcite ages from this study and published constraints on regional tectonic, volcanic, and basin evolution. Data sources (superscripts): 1—this study; 2—Diamond and Ingersoll (2002); 3—Oldow et al. (1994); 4—Darin et al. (2025); 5—Rangel et al. (2025); 6— Coffey et al. (2021) and Gagnon et al. (2023).

Clumped-isotope temperatures record pronounced variability in the thermal conditions of calcite precipitation across structural settings in Clayton Valley (**Figs. 3-5**), indicating that fluids likely circulated over a wide range of depths during basin evolution. Calcite mineralization along basin-bounding faults records the highest precipitation temperatures (139.2 °C and 104.6 °C), consistent with deep circulation along major fault systems. A similarly elevated temperature (135.6 °C) recorded by a basement-hosted vein is interpreted to reflect hydraulic connectivity to the basin-bounding fault system at depth. This vein is from Angel Island, and yielded a U-Pb age of 27.1 Ma, which is near the timing of onset of Basin and Range extension in the region. Angel Island is interpreted as a rider block above the regional Miocene detachment fault system – not exhumed from depth by the detachment faulting – as illustrated in Fig. 8. Calcite veins hosted in volcano–sedimentary units yield tightly clustered intermediate temperatures (~72 °C), whereas basement-hosted structures span the widest temperature range, from near-ambient (~20–31 °C) to the highest recorded values.

Near-ambient precipitation temperatures are strongly suggestive of shallow, meteoric-derived fluids. This interpretation is reinforced by sequential structural restoration of Clayton Valley (**Fig. 8a-d**), which places several low-temperature, lithium-bearing calcite veins at or near the Earth's surface at the time of mineralization (**Fig. 8b**). In contrast, coeval calcite veins that record higher temperatures occur on basin-bounding or subsidiary faults with clear access to deeper circulation levels, indicating that shallow meteoric and deeper hydrothermal systems operated contemporaneously within the basin.

Stable isotope compositions provide independent constraints on fluid source. Reconstructed fluid $\delta^{18}O$ values overlap the range of modern meteoric recharge, basin groundwater, and brines reported for Clayton Valley (**Fig. 6a**; Gagnon et al., 2023), while carbonate $\delta^{13}C$ values are substantially higher than typical mantle CO_2 signatures (~−5‰; Javoy et al., 1986). These isotopic signatures indicate dominantly meteoric, basin-buffered fluids and argue against a primary magmatic volatile contribution to

https://doi.org/10.5194/egusphere-2026-1596
Preprint. Discussion started: 1 April 2026

calcite mineralization. Elevated precipitation temperatures are therefore interpreted to reflect circulation depth and fluid–rock interaction along structurally focused pathways rather than direct magmatic fluid input.

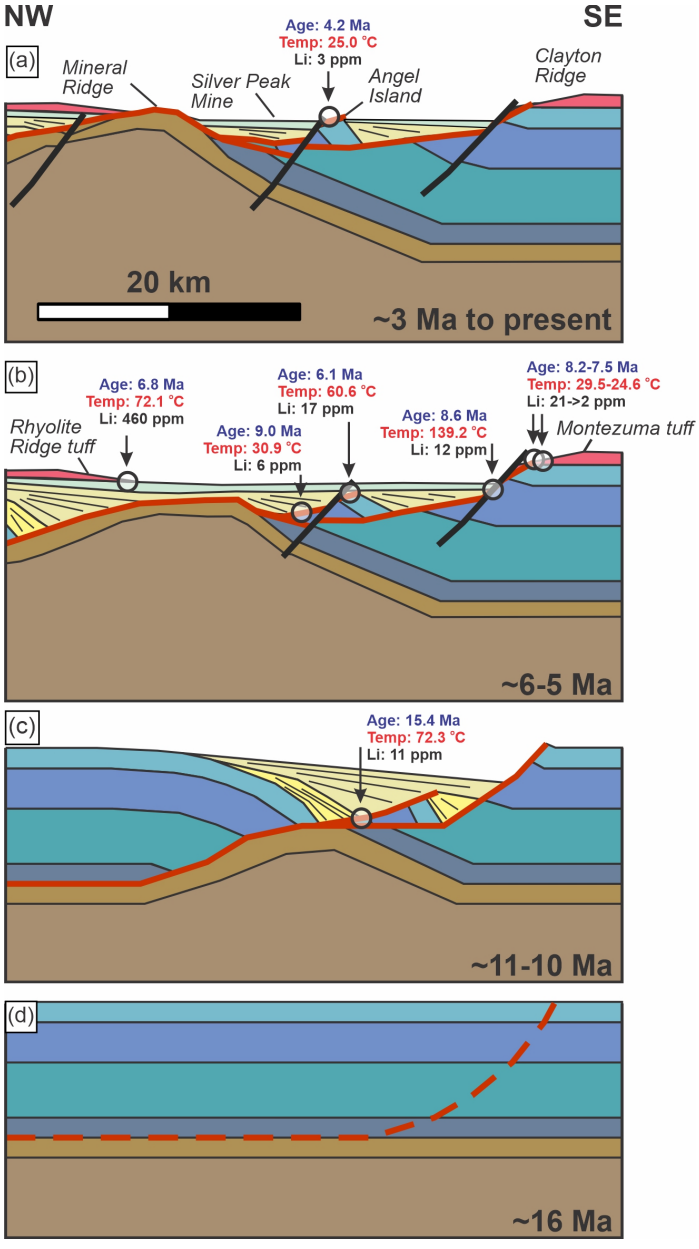

Figure 8. Schematic structural evolution of Clayton Valley at (a) ca. 3 Ma to present, (b) ca. 6-5 Ma, (c) ca. 11-1 Ma, and (d) ca. 16 Ma. Modified from Rangel et al. (2025). Vein calcite sample ages (blue), temperatures (red), and lithium concentrations (black) are shown relative to the evolving basin architecture. Samples are plotted at approximate time intervals when they are interpreted, based on U–Pb ages, to have already been present; panels do not imply fault initiation or mineralization at the illustrated times.

https://doi.org/10.5194/egusphere-2026-1596
Preprint. Discussion started: 1 April 2026

5.3 Structurally focused lithium transport in Clayton Valley

Lithium transport and redistribution in Clayton Valley are governed by basin-scale hydrologic processes and lithium availability, with fault and fracture networks likely acting to organize and enhance fluid connectivity and transport efficiency (e.g., Munk et al., 2016; Coffey et al., 2021; **Fig. 9**). Previous models have emphasized surface weathering of silicic volcanic units, catchment input, and evaporative concentration as primary controls on lithium delivery to the basin (**Fig. 9a**). Our results highlight the role of fault and fracture networks in enhancing the efficiency of lithium delivery by focusing fluids derived from surface weathering and shallow groundwater systems into fault-controlled pathways (**Fig. 9b-d**). Specifically, we provide evidence for (i) long-lived fault and fracture networks that transported lithium over multi-Myr timescales (**Figs. 7 and 8**), (ii) basinward lithium transport and associated advective circulation through fault and fracture networks, including downwelling of meteoric fluids and upwelling of warmer fluids during basin development (**Figs. 9b, 9c**), and (iii) structural connectivity also facilitates lithium exchange between basin-fill source intervals, ash- and tuff-hosted aquifers, and evolving brine reservoirs, improving the efficiency of leaching and redistribution processes previously invoked for basin-fill clays (**Fig. 9d**).

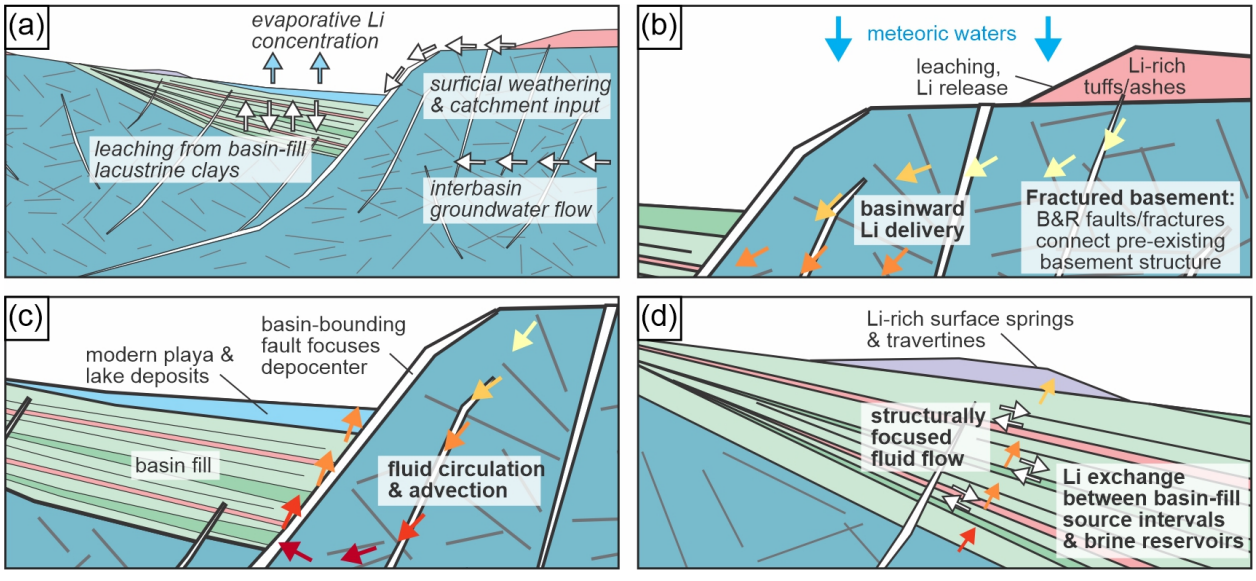

Figure 9. Conceptual model of structurally focused lithium transport and redistribution. (a) Previous workers' concepts of lithium transport and delivery at Clayton Valley (e.g., Coffey et al., 2021; Darin et al., 2025). (b) Linkage between basement and basin structures, leaching of lithium from silicic volcanic units, fault-controlled delivery of lithium-bearing fluids into developing basin accommodation space. (c) Advective circulation involving downwelling cooler fluids and upwelling warmer fluids. (d) Lithium exchange between basin-fill source intervals and brine reservoirs. B&R = Basin and Range.

The presence of Basin and Range–age structures that cross-cut and connect pre-existing brittle deformation fabrics and veins (e.g., **Fig. 2a, b**) highlights the propensity for these relatively late structures to link earlier deformation fabrics. These late structures would likely act as permeability backbones that connect fracture networks, enhancing basin-scale connectivity as fault systems grow, interact, and link (cf. Ferrill et al., 2017). In combination, these throughgoing, late-stage structures and connected early features would represent efficient flow pathways for fluids prior to mineralization or when only partially

https://doi.org/10.5194/egusphere-2026-1596
Preprint. Discussion started: 1 April 2026

mineralized. Long-range groundwater circulation has previously been proposed as a contributor to lithium enrichment in Clayton Valley, particularly as a mechanism for delivering solutes across basin boundaries (e.g., Munk et al., 2016). While our data do not uniquely require interbasin flow, the presence of lithium-bearing fluids prior to emplacement of major late Miocene silicic volcanic units indicates that lithium transport was already occurring within the basin before establishment of the most commonly cited volcanic source reservoirs. Our data potentially support a framework in which structurally connected fault networks enabled basin-scale or regional fluid circulation over long distances and geologic timescales.

Independent of the ultimate lithium source, the results here show that faults and fracture networks likely represent important components for groundwater flow and fluid connectivity within Clayton Valley over multi-Myr timescales. Our results are consistent with recent studies that link lithium enrichment to brittle deformation and faulting in extensional basins (e.g., Marazuela et al., 2020; Benson et al., 2023; Munk et al., 2025; Butler et al., 2025; Putzolu et al., 2025), but extend those interpretations by providing direct evidence that fault-mediated lithium transport can occur over million-year timescales. The combined timing, temperature, and isotopic data demonstrate that fault and fracture networks in Clayton Valley enabled long-lived, vertically extensive circulation of meteoric fluids, linking deep thermal regimes with basin fill and near-surface discharge zones. Regardless of lithium source, the data presented here show that long-lived fault and fracture networks may be important components of lithium transport and redistribution pathways in active closed-basin systems by focusing fluid flow, maintaining hydraulic connectivity through time, and enabling repeated internal redistribution of lithium during basin evolution.

6 Conclusions

Calcite veins and travertine deposits from Clayton Valley record multiple episodes of fluid flow associated with Basin and Range extension. Carbonate U–Pb ages indicate that mineralization occurred intermittently between ~15.4 and 3.9 Ma, demonstrating that structurally focused fluid flow persisted over multi-million-year timescales.

Lithium-bearing calcite precipitation occurred both before and after emplacement of late Miocene silicic volcanic units commonly cited as major lithium source reservoirs in the region. This temporal relationship shows that lithium-bearing fluids circulated repeatedly during basin evolution and that lithium transport was not uniquely tied to a single volcanic event or mineralizing episode.

Lithium concentrations vary with host setting, with higher values in basin-fill–hosted veins and travertine deposits and generally lower values in basement-hosted and basin-bounding fault veins. Clumped-isotope temperatures and stable isotope compositions indicate that lithium-bearing fluids were dominantly meteoric and reached elevated temperatures during circulation, indicating that lithium accumulation in Clayton Valley does not necessarily require lithium sourcing from magmatic fluids at depth.

https://doi.org/10.5194/egusphere-2026-1596
Preprint. Discussion started: 1 April 2026

Author contributions

Author contribution. AJC contributed to conceptualization, methodology, validation, formal analysis, investigation, data curation, visualization, writing – original draft, supervision, project administration, and funding acquisition. DAF contributed to conceptualization, formal analysis, investigation, writing – original draft, and funding acquisition. IAR-L contributed to conceptualization, methodology, and investigation. KLB contributed to conceptualization, investigation, and funding acquisition. DEI contributed to conceptualization, methodology, formal analysis, and investigation. ZTS contributed to conceptualization and funding acquisition. MRB contributed to investigation. BS contributed to investigation and/or domain expertise. KJS contributed to investigation and/or domain expertise. LAM contributed to conceptualization. DFB contributed to investigation and/or domain expertise. LDS contributed to methodology, formal analysis, and investigation. DFS contributed to investigation and/or domain expertise. CAG contributed to investigation and/or domain expertise. All authors (AJC, DAF, IAR-L, KLB, DEI, ZTS, MRB, BS, KJS, LAM, DFB, LDS, DFS, CAG) contributed to writing – review and editing and approved the final manuscript.

Competing interests

The authors declare that they have no conflicts of interest.

Acknowledgements

We thank Albemarle Corporation for data access and field support.

Financial support

Financial support provided by The University of Texas at Dallas Office of Research and Innovation and Southwest Research Institute® SPRINT program (15-R6492), and Southwest Research Institute® Internal Research and Development project 15-R6594

Supplement link

https://zenodo.org/records/18904592

References

Albers, J. P. and Stewart, J. H.: Geology and mineral deposits of Esmeralda County, Nevada, Nevada Bureau of Mines and Geology Bulletin, 78, 88 pp., 1972.

https://doi.org/10.5194/egusphere-2026-1596
Preprint. Discussion started: 1 April 2026

ALS: Geochemistry services – lithium, available at: https://www.alsglobal.com/en/geochemistry/energy-minerals-analysis/lithium (last access: 12 February 2025), 2025.

Anderson, N. T., Kelson, J. R., Kele, S., Daëron, M., Bonifacie, M., Horita, J., Mackey, T. J., John, C. M., Kluge, T., Petschnig, P., and Jost, A. B.: A unified clumped isotope thermometer calibration (0.5–1,100 °C) using carbonate-based standardization, Geophysical Research Letters, 48, e2020GL092069, 2021.

Bense, V. F., Gleeson, T., Loveless, S. E., Bour, O., and Scibek, J.: Fault zone hydrogeology, Earth-Science Reviews, 127, 171–192, 2013.

Benson, T. R., Coble, M. A., and Dilles, J. H.: Hydrothermal enrichment of lithium in intracaldera illite-bearing claystones, Science Advances, 9, eadh8183, 2023.

Bernasconi, S. M., Daëron, M., Bergmann, K. D., Bonifacie, M., Meckler, A. N., Affek, H. P., Anderson, N., Bajnai, D., Barkan, E., Beverly, E., and Blamart, D.: InterCarb: A community effort to improve interlaboratory standardization of the carbonate clumped isotope thermometer using carbonate standards, Geochemistry, Geophysics, Geosystems, 22, e2020GC009588, 2021.

Bhattacharya, T., Brennan, P. R., Ibarra, D. E., Gagnon, C. A., Butler, K. L., Terrazas, A., Miller, S., Munk, L. A., Boutt, D. F., Feng, R., and Bullinger, S. N.: Pleistocene shifts in Great Basin hydroclimate seasonality govern the formation of lithium-rich paleolake deposits, Quaternary Science Reviews, 335, 108747, 2024.

Bradley, D. C., Munk, L. A., Jochens, H., Hynek, S., and Labay, K. A.: A preliminary deposit model for lithium brines, U.S. Geological Survey Open File Report, 2013–1006, 2013.

Bradley, D. C., Stillings, L. L., Jaskula, B. W., Munk, L., and McCauley, A. D.: Lithium, in: Critical Mineral Resources of the United States—Economic and Environmental Geology and Prospects for Future Supply, edited by: Shultz, K. J., DeYoung, J. H., Seal, R. R., and Bradley, D. C., U.S. Geological Survey Professional Paper 1802, K1–K21, 2017.

Brand, W. A., Assonov, S. S., and Coplen, T. B.: Correction for the 17O interference in δ13C measurements when analyzing CO2 with stable isotope mass spectrometry (IUPAC Technical Report), Pure and Applied Chemistry, 82, 1719–1733, 2010.

Butler, K. L., Munk, L. A., Boutt, D. F., Morris, N., Kennedy, J., Saha, P., Blake, M. R., Custado, M. J., and Ibarra, D. E.: The origin and enrichment of sedimentary basin lithium brines: A case study from the Upper Devonian Leduc Formation, Alberta Basin, Canada, Economic Geology, 120, 649–662, 2025.

Caine, J. S., Evans, J. P., and Forster, C. B.: Fault zone architecture and permeability structure, Geology, 24, 1025–1028, 1996.

Cawood, A. J., Ferrill, D. A., Morris, A. P., Norris, D., McCallum, D., Gillis, E., and Smart, K. J.: Tectonostratigraphic evolution of the Orphan Basin and Flemish Pass region – Part 1: Results from coupled kinematic restoration and crustal area balancing, Marine and Petroleum Geology, 128, 105042, 2021.

Cawood, A., Ferrill, D., Rangel-Landeros, I., Butler, K., Sickmann, Z., Blake, M., Ibarra, D., Swanson, B., Munk, L., Boutt, D., Stockli, L., Stockli, D., and Gagnon, C.: Geochemical constraints on lithium transport in fault and fracture systems, Geological Society of America Abstracts with Programs, 57, 272-9, 2025.

https://doi.org/10.5194/egusphere-2026-1596
Preprint. Discussion started: 1 April 2026

Cawood, A. J.: Supplemental data for "Long-lived lithium transport through fault and fracture networks in Clayton Valley, Nevada", Zenodo [data set], 2026.

Chen, T. W., Smye, A., Lloyd, M., Fisher, D., and Hashimoto, Y.: Temperatures of vein formation associated with plate interface deformation constrained by oxygen and clumped isotope thermometry, Geochemistry, Geophysics, Geosystems, 25, e2024GC011516, 2024.

Chew, D. M., Petrus, J. A., and Kamber, B. S.: U–Pb LA–ICP–MS dating using accessory mineral standards with variable common Pb, Chemical Geology, 363, 185–199, 2014.

Coffey, D. M., Munk, L. A., Ibarra, D. E., Butler, K. L., Boutt, D. F., and Jenckes, J.: Lithium storage and release from lacustrine sediments: Implications for lithium enrichment and sustainability in continental brines, Geochemistry, Geophysics, Geosystems, 22, e2021GC009916, 2021.

Daëron, M., Blamart, D., Peral, M., and Affek, H. P.: Absolute isotopic abundance ratios and the accuracy of Δ47 measurements, Chemical Geology, 442, 83–96, 2016.

Diamond, D. and Ingersoll, R.: Structural and sedimentologic evolution of a Miocene supradetachment basin, Silver Peak Range and adjacent areas, west-central Nevada, International Geology Review, 44, 588–623, 2002.

Darin, M. H., Harlaux, M., Ogilvie, I. A., Reynolds, J. T., and Chafetz, D. A.: Source-to-sink evolution of volcano-sedimentary Li–B deposits at Rhyolite Ridge, southwestern Nevada, Economic Geology, 120, 1167–1190, 2025.

Davis, J. R. and Vine, J. D.: Stratigraphic and tectonic setting of the lithium brine field, Clayton Valley, Nevada, Rocky Mountain Association of Geologists Basin and Range Symposium, 421–430, 1979.

Davis, J. R., Friedman, I., and Gleason, J. D.: Origin of the lithium-rich brine, Clayton Valley, Nevada, U.S. Geological Survey Bulletin, 1622, 131–138, 1986.

Davis, G. H., Bos Orent, E., Clinkscales, C., Ferroni, F. R., Gehrels, G. E., George, S. W. M., et al.: Structural analysis and chronologic constraints on progressive deformation within the Rincon Mountains, Arizona: Implications for development of metamorphic core complexes, Geological Society of America Memoir, 222, 1–125, 2023.

Drake, H., Mathurin, F. A., Zack, T., Schäfer, T., Roberts, N. M., Whitehouse, M., Karlsson, A., Broman, C., and Åström, M. E.: Incorporation of metals into calcite in a deep anoxic granite aquifer, Environmental Science & Technology, 52, 493–502, 2018.

Eaton, G. P.: The Basin and Range province: Origin and tectonic significance, Annual Review of Earth and Planetary Sciences, 10, 409–440, 1982.

Ferrill, D. A., Morris, A. P., McGinnis, R. N., and Smart, K. J.: Myths about normal faulting, Geological Society, London, Special Publications, 439, 41–56, 2017.

Ferrill, D. A., Smart, K. J., Cawood, A. J., and Morris, A. P.: The fold-thrust belt stress cycle: Superposition of normal, strike-slip, and thrust faulting deformation regimes, Journal of Structural Geology, 148, 104362, 2021.

Fyfe, W. S., Price, N. J., and Thompson, A. B.: Fluids in the Earth's crust, Elsevier, Amsterdam, 1978.

https://doi.org/10.5194/egusphere-2026-1596
Preprint. Discussion started: 1 April 2026

Gagnon, C. A., Butler, K. L., Gaviria, E., Terrazas, A., Gao, A., Bhattacharya, T., Boutt, D. F., Munk, L. A., and Ibarra, D. E.: Paleoclimate controls on lithium enrichment in Great Basin Pliocene–Pleistocene lacustrine clays, Geological Society of America Bulletin, 135, 3201–3212, 2023.

Ghosh, P., Adkins, J., Affek, H., Balta, B., Guo, W., Schauble, E. A., Schrag, D., and Eiler, J. M.: 13C–18O bonds in carbonate minerals: A new kind of paleothermometer, Geochimica et Cosmochimica Acta, 70, 1439–1456, 2006.

Guillong, M., Samankassou, E., Müller, I. A., Szymanowski, D., Looser, N., Tavazzani, L., Merino-Tomé, Ó., Bahamonde, J. R., Buret, Y., and Ovtcharova, M.: Technical note: RA138 calcite U–Pb LA-ICP-MS primary reference material, Geochronology, 6, 465–474, 2024.

Hancock, P. L.: Brittle microtectonics: Principles and practice, Journal of Structural Geology, 7, 437–457, 1985.

Heilweil, V. M. and Brooks, L. E. (eds.): Conceptual model of the Great Basin carbonate and alluvial aquifer system, U.S. Geological Survey Scientific Investigations Report 2010–5193, 191 pp., 2011.

Hollocher, K. and Ruiz, J.: Major and trace element determinations on NIST glass standard reference materials by inductively coupled plasma mass spectrometry, Geostandards Newsletter, 19, 27–34, 1995.

Javoy, M., Pineau, F., and Delorme, H.: Carbon and nitrogen isotopes in the mantle, Chemical Geology, 57, 41–62, 1986.

Jochum, K. P., Willbold, M., Raczek, I., Stoll, B., and Herwig, K.: Chemical characterisation of USGS reference glasses using multiple techniques, Geostandards and Geoanalytical Research, 29, 285–302, 2005.

Kaiyun, C., Honglin, Y., Zhian, B., Chunlei, Z., and Mengning, D.: Precise in situ determination of lead isotope ratios using femtosecond laser ablation MC-ICP-MS, Geostandards and Geoanalytical Research, 38, 5–21, 2014.

Kunasz, I. A.: Lithium occurrence in the brines of Clayton Valley, Esmeralda County, Nevada, Proceedings of the Fourth Symposium on Salt, 57–66, 1974.

Munk, L., Jochens, H., Jennings, M., Bradley, D., Hynek, S., and Godfrey, L.: Geochemistry of lithium-rich brines in Clayton Valley, Nevada, Proceedings of the 11th SGA Biennial Meeting, 217–219, 2011.

Munk, L. A., Hynek, S. A., Bradley, D., Boutt, D. F., Labay, K., and Jochens, H.: Lithium brines: A global perspective, Reviews in Economic Geology, 18, 339–365, 2016.

Munk, L. A., Boutt, D., Butler, K., Russo, A., Jenckes, J., Moran, B., and Kirshen, A.: Lithium brines: Origin, characteristics, and global distribution, Economic Geology, 120, 575–597, 2025.

Marazuela, M. A., Ayora, C., Vázquez-Suñé, E., Olivella, S., and García-Gil, A.: Hydrogeological constraints for lithium enrichment in the Salar de Atacama, Science of the Total Environment, 739, 139959, 2020.

Noble, D. C., Anderson, R. E., Ekren, E. B., and O'Connor, J. T.: Thirsty Canyon Tuff of Nye and Esmeralda Counties, Nevada, U.S. Geological Survey Professional Paper 475-D, D24–D27, 1964.

Oldow, J. S., Kohler, G., and Donelick, R. A.: Late Cenozoic extensional transfer in the Walker Lane strike-slip belt, Nevada, Geology, 22, 637–640, 1994.

Oldow, J. S., Geissman, J. W., and Stockli, D. F.: Evolution of late Neogene transtension in structural stepovers linking the Walker Lane and Eastern California Shear Zone, International Geology Review, 50, 1–21, 2008.

https://doi.org/10.5194/egusphere-2026-1596
Preprint. Discussion started: 1 April 2026

Palacios-García, N. B., Fitz-Díaz, E., Stockli, L. D., and Stockli, D. F.: U–Pb calcite dating of brittle deformation in Permian carbonates, Journal of Structural Geology, 171, 104863, 2023.

Paton, C., Hellstrom, J., Paul, B., Woodhead, J., and Hergt, J.: Iolite: Freeware for the visualisation and processing of mass spectrometric data, Journal of Analytical Atomic Spectrometry, 26, 2508–2518, 2011.

Price, J. G., Lechler, P. J., Lear, M. B., and Giles, T. F.: Possible volcanic sources of lithium in Clayton Valley, Nevada, Geological Society of Nevada Symposium Proceedings, 241–248, 2000.

Putzolu, F., Armstrong, R. N., Benson, T. R., Boutt, D. F., Butler, K. L., Dolgopolova, A., Herrington, R. J., Ibarra, D. E., and Munk, L. A.: Volcano-sedimentary deposits: Overview of an emerging type of lithium resource, Economic Geology, 120, 541–573, 2025.

Rangel, I., Cawood, A., Butler, K., Sickmann, Z., Blake, M., Swanson, B., Ibarra, D., Gagnon, C., Munk, L., Boutt, D., Ferrill, D., and Smart, K.: Revised tectonic framework for the Clayton Valley lithium deposits, Geological Society of America Abstracts with Programs, 57, 272-3, 2025.

Roberts, N. M. and Walker, R. J.: U–Pb geochronology of calcite-mineralized faults, Geology, 44, 531–534, 2016.

Roberts, N. M., Rasbury, E. T., Parrish, R. R., Smith, C. J., Horstwood, M. S., and Condon, D. J.: A calcite reference material for LA-ICP-MS U–Pb geochronology, Geochemistry, Geophysics, Geosystems, 18, 2807–2814, 2017.

Stewart, J. H.: Regional characteristics, tilt domains, and extensional history of the Basin and Range province, Geological Society of America Special Paper 323, 47–74, 1998.

Stewart, J. H. and Diamond, D. S.: Changing patterns of extensional tectonics, Geological Society of America Memoir 176, 447–475, 1990.

Tera, F. and Wasserburg, G. J.: U–Th–Pb systematics in lunar highland samples, Earth and Planetary Science Letters, 17, 36–51, 1972.

Thompson, A. L., Richardson, C. A., Gootee, B. F., Wilkins, J., and Fenerty, B.: Geology, geochemistry, and potential origins of the Basin volcano-sedimentary lithium deposit, Economic Geology, 120, 663–688, 2025.

U.S. Geological Survey: Quaternary fault and fold database for the United States, available at: https://www.arcgis.com/apps/webappviewer/index.html?id=5a6038b3a1684561a9b0aadf88412fcf (last access: 31 December 2024), 2024.

Vermeesch, P.: IsoplotR: A free and open toolbox for geochronology, Geoscience Frontiers, 9, 1479–1493, 2018.

Watts, K. E.: Lithium from magma to mine in an early Yellowstone hotspot caldera, Geology, 53, 592–596, 2025.